Received: 17 May 2021 | Revised: 21 June 2021 | Accepted: 9 July 2021

DOI: 10.1002/arp.1841

RESEARCH ARTICLE

WILEY

Practical considerations for shallow submerged archaeological prospection with 3-D electrical resistivity tomography

Nikos Papadopoulos[1] | Dimitrios Oikonomou[1] | Kleanthis Simyrdanis[1] | Loke Meng Heng[2]

[1]GeoSat ReSeArch Lab, Institute for Mediterranean Studies–Foundation for Research and Technology Hellas, Rethymno, Crete, Greece

[2]Geotomo Software Sdn Bhd, Gelugor, Penang, Malaysia

Correspondence
Nikos Papadopoulos, GeoSat ReSeArch Lab, Institute for Mediterranean Studies–Foundation for Research and Technology Hellas, Nik., Foka 130, Rethymno, Crete. Greece.
Email: nikos@ims.forth.gr

Funding information
Operational Programme "Crete 2014–2020"; European Regional Development Fund

Abstract

Direct current electrical resistivity method has experienced significant breakthroughs during the last decades with the development of advanced instrumentation and sophisticated inversion algorithms. These have substantially benefitted the field of archaeological prospection to extract quantitative information for the buried archaeological material in a complete three-dimensional (3-D) context. The obvious continuation of past human occupation and associated settlements in the ultra-shallow part of coastal zones generated the necessity to compile methodologies for mapping submerged cultural assets. This study investigates the efficiency of dynamic floating and submerged 3-D Electrical Resistivity Tomography (ERT) for mapping archaeological relics buried beneath the sediments in ultra-shallow marine environments. Extensive testing is performed through numerical simulation and 3-D inversion of synthetic apparent resistivity tomographic data. The generic resistivity model including a complex resistive structure embedded in a stratified conductive environmental regime simulated typical scenario of an archaeological feature submerged below the sea water layer. Different array configurations including Dipole–Dipole (DD), Gradient (GRD), Reciprocal Wenner (RecWEN) and Wenner-Schlumberger (WS), which can be appropriately programmed for continuous off-shore measurements with associated multichannel resistivity instruments, are validated in order to determine the most efficient one for such surveys. Densely spaced multiple parallel two-dimensional (2-D) ERT lines along a single direction composed the survey layout to extract the 3-D apparent resistivity data set for the different electrode arrays using a 3-D finite element program. The synthetic tomographic data were corrupted with 3% Gaussian noise and inverted with an iterative smoothness constrained inversion algorithm. The comparative results from the various tested arrays manifest the superiority of the DD in reconstructing the optimum resistivity inversion model for both the floating and submerged survey modes. Additional tests were made concerning the resolving capabilities of ERT with variable seawater thickness and target characteristics. Although accurate 'a priori' information regarding the water resistivity and thickness are essential for constraining the 3-D inversion, erroneous estimation of these parameters can result to misleading results, especially for submerged survey modes. The simulation of floating and submerged 3-D ERT surveys through synthetic modelling documented the benefits of such approach in reconstructing structured cultural

material in shallow off-shore environments. Finally, the results of a 3-D dynamic floating ERT survey from a submerged archaeological site in Greece verified the theoretical outcomes, proposing at the same time techniques to overcome problems that can occur due to the unique conditions of the ultra-shallow marine environment. Overall, this work enhances the conclusion that 3-D marine ERT is a robust method to reconstruct submerged archaeological structures related to ancient built environment in ultra-shallow marine regions.

KEYWORDS
3-D inversion, archaeology, modelling, resistivity

1 | INTRODUCTION

The direct current resistivity survey method was pioneered more than a century ago (Schlumberger, 1912). The last three decades substantial advancements of the method included the construction of new multielectrode/multichannel systems (Imaduddi et al., 2019) and the compilation of automated reconstruction algorithms able to run in microcomputers (M.H. Loke & Barker, 1996). Thus, nowadays, resistivity prospection is widely used to image buried targets ranging from millimetre to kilometre scale.

The additional research in the field of developing experimental procedures to generate optimized array protocols that carry higher resolving power and exhibit larger investigation depth than commonly used electrode configurations, pushed further resistivity method to image and monitor the subsurface geoelectrical properties (Stummer et al., 2004). Thus, the efficient completion of 2-D, 3-D and even 4-D electrical resistivity tomography (ERT) surveys for solving hydrogeological, environmental, engineering and mining problems was made feasible, illuminating the subsurface complexity which otherwise would not be possible with traditional 1-D field and interpretation approaches (M.H. Loke et al., 2013). Inevitably, within the last two decades, these aforementioned innovations enriched archaeological geophysics with specific developments and numerous applications of ERT, in imaging and reconstructing the hidden built and natural archaeoenviornment in diverse landscapes (Arato et al., 2015; Osella et al., 2005; N. Papadopoulos, 2019; Szalai et al., 2011; Vafidis et al., 1999; Yilmaz et al., 2019).

A complete 3-D survey involves the distribution of the electrodes in regular or arbitrary positions in space, measuring the potential differences along all possible directions (M.H. Loke & Barker, 1996). One of the earliest efforts of 3-D ERT in archaeological applications involved the physical image reconstruction of subsurface resistivity discontinuities in a probabilistic sense (Di Fiore et al., 2002; Mauriello et al., 1998). Although this approach can handle the subsurface resistivity complexity, it is not practical even today for routine applications due to the limitation imposed by the logistics. Thus, the geophysical community placed a substantial research effort to define alternative efficient survey strategies and optimum processing flowcharts to image the archaeological structures in a complete 3-D context. The reconstruction of cultural assets like buildings, tombs, multilayer settlements and burial mounds was based on the collection of 3-D data sets composed of a series of static parallel (Al-Saadi et al., 2018; Cifuentes-Nava et al., 2013; Drahor et al., 2007; N.G. Papadopoulos et al., 2006, 2007, 2010) or radial 2-D lines (Chen et al., 2018; Tsourlos et al., 2014), accompanied by the implementation of 3-D resistivity inversion algorithms.

In urbanized environments with limited space to deploy parallel lines, the apparent resistivity can be captured form 'L'- and 'corner'-shaped profiles that surround surface obstacles. Tejero-Andrade et al. (2015) investigated the resolving capabilities of such techniques using heuristic rules for choosing the electrode configurations. The results with synthetic and real data signified the sensitivity of such deployments for deeper objects and the respective lower resolution for shallower resistive anomalies. Abdullah et al. (2019) made a step further to the specific concept, defining optimized configurations that maximize the model resolution along the perimeter of a confined area.

The development of computerized mobile quadripoles contributed in the extensive mapping of large areas combining high spatial resolution and reduction in survey time (Panissod et al., 1997). The Automatic Resistivity Profiling (ARP) comprised a specific variant of such a dynamic system allowing continuous measurements over several depths of investigation, in order to perform an exhaustive 3-D geoelectrical exploration (Dabas, 2008). N.G. Papadopoulos et al. (2009) explored the limitations and possibilities of the 3-D resistivity inversion of ARP data signifying its complementarity in the quantitative interpretation of the buried archaeological features. In areas with extreme resistive surface materials, where it is difficult to use conventional resistivity metres to inject the galvanic current into the subsurface, dynamic capacitively coupled systems can be used for rapid 3-D coverage (O. Kuras et al., 2007, 2018).

The continuous evolvement of fully automated algorithms for the 3-D inversion of resistivity data also benefited the efficient mapping of the archaeolandscape. The collection of high-resolution 3-D tomographic data generated the necessity of proposing fast inversion methodologies, minimizing the computer memory requirements. Brinon et al. (2012) presented a two-step approach by first fitting a 1-D electric model on the data over the entire surveyed area and

subsequent localized 3-D interpretation to enhance the information context of specific features. N.G. Papadopoulos et al. (2011) proposed a fast and memory efficient 3-D inversion algorithm using geometric criteria to calculate the significant part of the sensitivity matrix and an iterative routine to solve the least squares equations. Gündogdu and Candansayar (2018) published a comprehensive study with numerical modelling and a real example from a Turkish archaeological site regarding the effects of different stabilizers on the 3-D resistivity tomographic inversion.

Moving on, a different environment waterborne resistivity surveys in areas covered with either brackish or saline water involve a number of electrodes attached on the water bottom or on a streamer towed by a boat to log high density and quality data. The accurate interpretation of such data sets poses new challenges in terms of processing flowcharts, because the conductive nature of the water layer has a significant effect in the actual resistivity measurements that must be incorporated in any modelling procedure (Baumgartner, 1996; Lagabrielle, 1983; M.H. Loke et al., 2019; M.H. Loke & Lane, 2004).

The literature includes a number of diverse ERT investigations in aquatic environments like the mapping of water bed sediments (Orlando, 2013; Sumintadireja & Irawan, 2016; Yang et al., 2002), the delineation of fracture zones inside resistive bedrock (Tassis et al., 2020) and the correlation of sub bottom geological formations with inverted resistivity (Psomiadis et al., 2009; D.F. Rucker et al., 2011). The geotechnical characterization of submerged lithological formations prior the construction of infrastructures (Dahlin & Loke, 2018; Kwon et al., 2005; D.F. Rucker & Noonan, 2013), the parametric evaluation of groundwater-seawater interactions (Carretero et al., 2019) and the monitoring of artificial solute tracers within streambed sediments (Clemenence et al., 2017) also show the variability of such surveys. Lee et al. (2018) presented a comprehensive methodology for the real time tracking of underwater moving objects in relatively large investigation depths as a complementary approach to acoustic methods.

2 | THREE-DIMENSIONAL ERT IN AQUATIC ENVIRONMENTS: NUMERICAL MODELLING AND INVERSION

Nowadays ERT investigations comprise an integral part of any archaeological project, mapping on-shore buried cultural antiquities in a non-destructive manner. However, this technology had so far minimal contribution towards the understanding of the past dynamics in ultra-shallow wetland environments. K. Simyrdanis et al. (2015) presented the first systematic effort to investigate the efficiency of ERT in imaging isolated submerged structural remains in very shallow saline water environments based on synthetic modelling and field experiments. Loddo et al. (2016) outlined some methodological issues on the applicability of 2-D ERT for archaeological prospection in shallow marine environments. Fediuk et al. (2020) investigated the measurement uncertainty and sensitivity of the inverse Schlumberger for reconstructing the submerged resistivity using 1-D and 2-D numerical models and field measurements.

ERT was also successful to outline submerged shipwrecks using quasi-3-D or full 3-D inversion processing approaches, through its lower resistivity signature with respect to saline or brackish water background, using towed floating mobile arrays (Passaro, 2010) or static submerged modes (K. Simyrdanis et al., 2018). Bouchette et al. (2014) studied the applicability of 3-D electrical impedance tomography for underwater applications completing experiments in a small water tank and sinking different objects in various horizontal and vertical positions. K. Simyrdanis et al. (2016) investigated the part of the Hellenistic submerged archaeological site of Olous in Crete (Greece) through a dense network of closely spaced submerged static ERT lines.

It is evident that the underwater environment provides an almost ideal case for resistivity surveying because there is no problem in obtaining good electrode contact. The implementation of a 3-D ERT survey in water-covered areas follows similar guidelines as in the case of 2-D submerged resistivity imaging. The measuring modes can be classified in two main categories that differ in the installation of the electrodes, either floating on the water surface or being in direct contact with the sea-bottom.

Both alternatives can be combined with a stationary or a dynamic configuration. Stationary variant involves the anchoring of the multimode electrode cable between two fixed positions, maintaining the stability of the array throughout the tomographic data collection along different lines. On the contrary, mobile surveys include the towing of the electrode cable behind a boat with steady speed to gather continuous 2-D scans along predefined transects.

The choice of submerged or floating survey modes depends mainly on the water column thickness, the variations of the seabed and the properties of the submerged targets. Floating dynamic systems have the obvious advantage of faster surveying speed and extensive area coverage. However, in shallow archaeological sites, submerged modes (static or dynamic) are preferable for mapping isolated archaeological structures, because they can efficiently account for the effect of the conductive sea layer (K. Simyrdanis et al., 2015).

The purpose of this work is to extract the resolving properties of arrays that are suitable for submerged or floating dynamic ERT measurements using any modern multichannel resistivity instrumentation. This study will test electrode configurations able to measure simultaneously the potential differences in multiple receiving pairs with a single current injection. Figure 1 shows schematically the electrode layouts for Dipole–Dipole (DD), Gradient (GRAD), reciprocal Wenner (RecWEN) and Wenner-Schlumberger (WS) using a cable with totally 13 equidistant take-outs, where two of them are used as current sources and the potential measurements are made on the remaining 11 electrodes. The cable is towed behind a boat moving with a specific speed, collecting successively 10 resistivity measurements with increasing distance between the potential and current dipoles, gradually covering the subsurface stratigraphy along a continuous 2-D dynamic line. Ultimately, the 3-D imaging of the resistivity properties

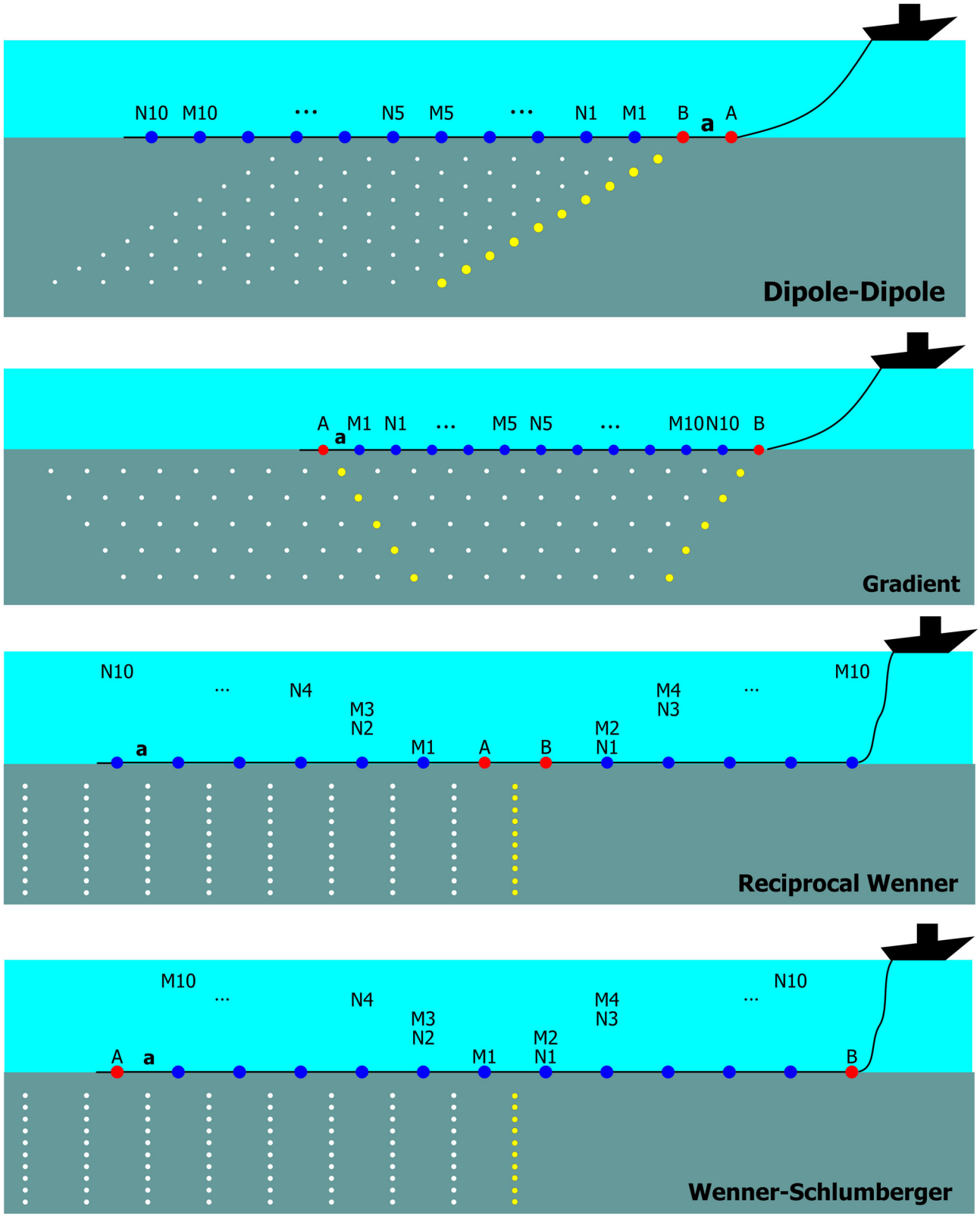

FIGURE 1 Schematic representation of the different electrode arrays that are tested in this work for dynamic ERT survey. A streamer cable for a 10-channel resistivity instrument is used where the potential measurements are logged in 11 electrodes (blue dots) with a single current injection from the two source points (red dots). The unit electrode distance between the 13 electrodes is $a = 1$ m. The white dots indicate the relative position of the apparent resistivity data, whereas the yellow dots show the respective measurements from a specific current injection [Colour figure can be viewed at wileyonlinelibrary.com]

below the seabed was facilitated through the completion of multiple similar 2-D lines along a specific direction (Figure 2).

The 3-D resistivity model in Figure 3 simulates a two layer stratigraphy below the water surface confined within a modelling space of 20 m × 15 m × 5 m in the *X*, *Y* and *Z* directions, respectively. The value of 0.2 Ohm-m was assigned to the saline water layer and the resistivity of the submerged layers gradually increases from 1 to 10 Ohm-m. The first submerged layer is 2.5 m thick and lies exactly below the seabed. This layer hosts a rectangular prism with resistivity 5 Ohm-m and 1-m thickness that represents the relics of a complex building with inner compartments separated by small walls, occupying a total area of 7 m by 5 m. The thickness of the conductive water layer was variable to evaluate its effect in the inversion images. The rectangular prism could be placed in different depths below the seabed to test the vertical and horizontal resolving capabilities of the floating or submerged aquatic resistivity investigation. The outline and the actual horizontal and vertical position of the structure are indicated with a solid line in the respective inversion model depth slices.

The 336 electrodes were evenly distributed on the nodes of a 20 m by 15 m rectangular area with 1 m spacing in both the *X* and *Y* directions. The DD, GRAD, RecWEN and WS array measurements along a single 2-D profile were taken with the explicit layout shown in Figure 1, using a current dipole and 10 receiving dipoles for each one of the different electrode configurations. The data sets describing the 3-D apparent resistivity variation for DD, GRAD, RecWEN and WS included 2,160, 1,440, 1,350 and 1,440 points, respectively, after merging 16 dynamic parallel 2-D lines along the *X* direction.

The program RES3DMODx64 (M.H. Loke, 2014) was the basis to calculate the response of the resistivity models for specific electrode configurations and extract the synthetic apparent resistivity data with a 3-D finite element solver. The forward modelling mesh had 100, 80 and 15 nodes in the *X*, *Y* and *Z* directions. Four mesh lines were used between the electrodes to give more accurate results and extra 10 nodes at the sides of the mesh along the *X* and *Y* directions, with progressively increasing spacing, to simulate the infinite distance from the sources. Out of the 15 vertical nodes, nine were used for eight model layers, either below the water surface or below the seabed, depending on actual measuring mode. The simulation of the floating survey mode was made feasible by assigning the water resistivity of 0.2 Ohm-m to one or more of the eight model layers. On the contrary, for the submerged mode an extra superficial model layer with variable thickness was used to assign the fixed water resistivity. The simulated synthetic tomographic apparent resistivity data for the different electrode arrays were corrupted with 3% Gaussian noise on the modelled apparent resistivity values.

The model grid used for the data inversion had 20 by 15 cells with 1 m width in both the *X* and *Y* directions and eight layers 0.5 m

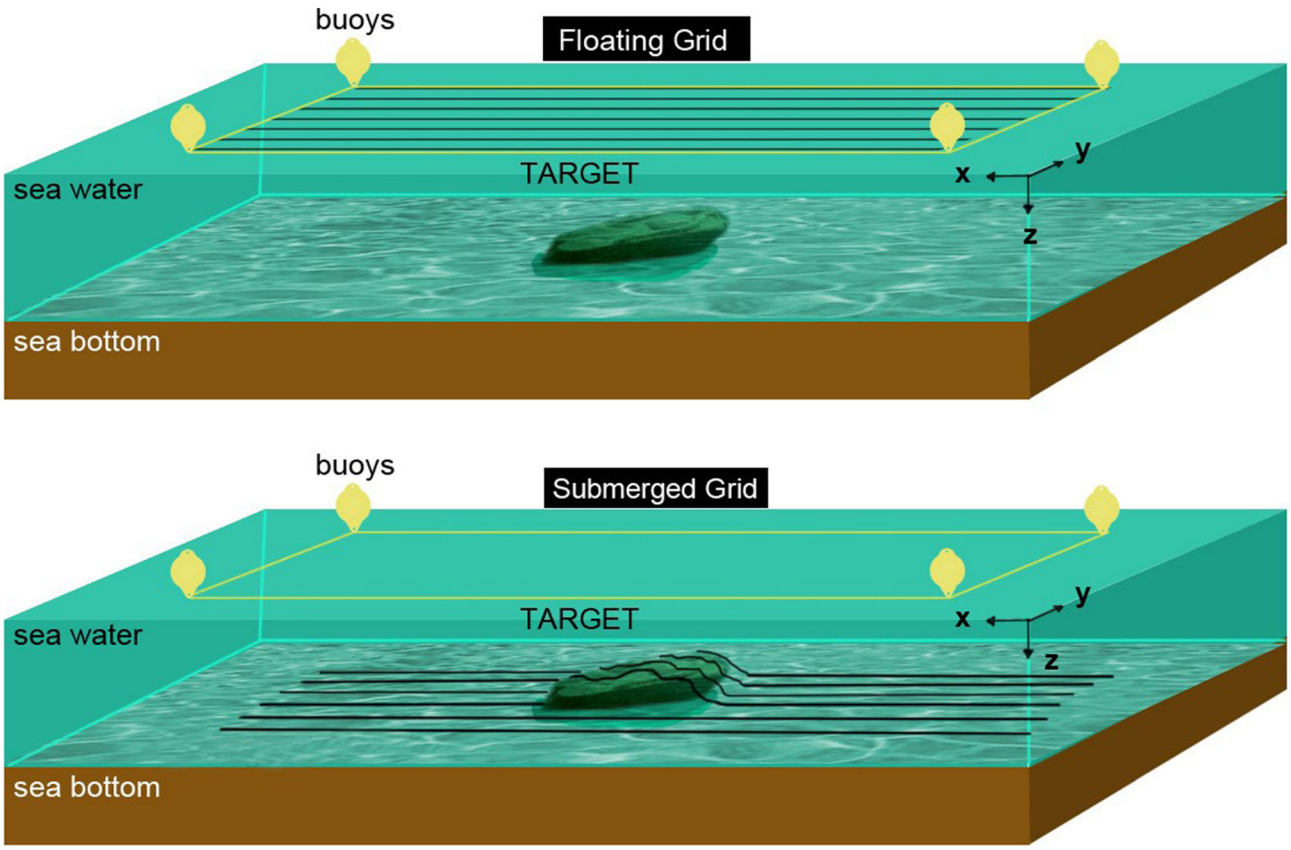

FIGURE 2 Illustration of a 3-D floating or submerged marine ERT survey along a dense grid of parallel 2-D lines [Colour figure can be viewed at wileyonlinelibrary.com]

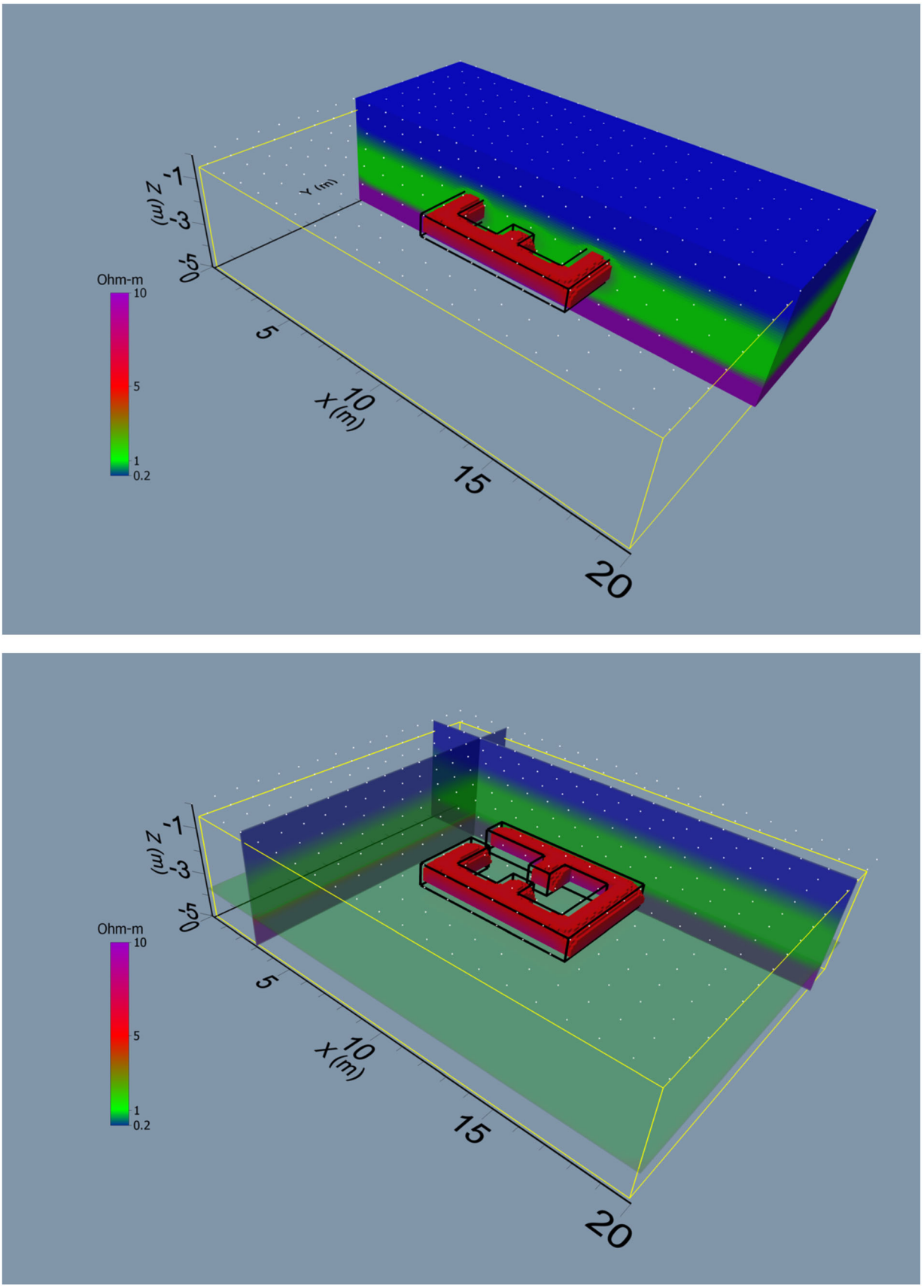

FIGURE 3 Resistivity model in three dimensions showing the saline water layer and a stratified medium below the seabed. The layer below the seabed includes a resistive prism that simulates the remains of a submerged archaeological structure [Colour figure can be viewed at wileyonlinelibrary.com]

thick each, giving a total of 2,400 model cells. For the 3-D inversion, RES3DINVx64 (M.H. Loke, 2017) was used to reconstruct the submerged resistivity model employing an iterative smoothness constrained least squares optimization algorithm. The resistivity estimate x_{k+1} at the $k+1$th iteration is given by

$$x_{k+1} = x_k + dx_k = x_k + \left[\left(J_k{}^T J_k + \lambda_k C^T C\right)\right]^{-1} J_k{}^T [y - F(x_k)], \quad (1)$$

where y is the measured data vector with the apparent resistivity values (logarithm), J_k is the Jacobian matrix estimate that contains the partial derivatives of the measured data (logarithm of apparent resistivity) with respect to the logarithm of the model resistivity, dx_k is the model resistivity (logarithm) correction vector, $F(x_k)$ is the forward modelling operator that calculates the response of a resistivity model, C is the stabilizing matrix which describes the smoothness pattern of the model (deGroot-Hedlin and Constable, 1990) and λ_k the Lagrangian multiplier that balances data misfit and model roughness. The inversion algorithm terminated when a specific number of iterations was reached (5–6) or the root mean square error (RMS) between the real and modelled apparent resistivity data was below a given threshold based on the estimated data noise (e.g., 3%).

In aquatic surveys, the seawater and the seabed comprise a distinct interface with rapid and sharp resistivity change across this boundary. Thus, the thickness and the resistivity of the saline water layer are crucial parameters that need to be measured with accuracy and included in the modelling and inversion procedure. For the case of floating aquatic surveys, the first modelling layer (out of the eight) was used to assign the seawater resistivity value and constrain the inversion and the depth resistivity slices in this case referred below the surface of the water. On the other hand, an extra superficial modelling layer was added for the inversion of the submerged ERT data to account for the effect of the water medium and the plots in this case referred below the sea bottom.

3 | INVERSION RESULTS

3.1 | Comparison of different electrode configurations and floating versus submerged mode

Previous, 2-D ERT numerical and experimental results showed that floating survey modes are quite successful to map isolated archaeological structures in relative shallow marine environments, where the water layer is less than 1 m thick (K. Simyrdanis et al., 2015). Thus, in order to test the efficiency of the different floating electrode arrays in mapping underwater structural objects, a thickness of 0.5 m was used for the saline water layer.

Figure 4 shows the first four inverted resistivity depth slices, up to the depth of two meters below the water surface, which were extracted from the respective 3-D inversion models for the floating DD, GRAD, RecWen and WS arrays. The modelling and inversion procedure was constrained by assigning the known resistivity value of 0.2 Ohm-m to the first modelling layer. After five iterations, the models from all the different arrays exhibited comparable RMS errors (2.74–2.85%), but the respective resistivity distributions showed distinct differences.

The DD model exhibits the optimum reconstruction of the shape, the small vertical walls and the thickness of the structure in the depth slices of 0.5–1.5 m (Figure 4a). GRAD array shows the general outline of the prism in the second and the third depth slices, but it was not capable to extract finer details like the small vertical segments that divided the submerged structure into two main compartments (Figure 4b). RecWen seems to faintly track the small walls oriented vertically to the direction of the survey lines, showing at the same time strong linear inversion artefacts at the left and right sides of the model due to insufficient data coverage (Figure 4c). WS was the least successful because the inversion model shows unformatted and compact resistivity signature in the position of the buried structure (Figure 4d).

A slightly harder environment using a thicker water layer (1 m) was used to compare the inversion models from the different arrays for the submerged mode. The resistivity depth slices below the sea bottom for the respective electrode configurations are shown in Figure 5. Although the DD generated the largest RMS error (3.12%) among all the other reconstructed models, it was the most successful in extracting the actual quantitative attributes of the submerged structure within the depth of 1 m below the sea bottom (Figure 5a). GRAD and RecWen depth slices have comparable resistivity images giving a bulk representation of the submerged feature without any finer resolution (Figure 5b,c). The insufficient lateral data coverage for the RecWen is attributed with the vertical linear resistive artefacts in the respective depth slices (Figure 5c). As in the case of the floating mode, WS was the least effective in imaging the size and the dimensions of the structure (Figure 5d).

The general comparison between the floating (Figure 4) and submerged (Figure 5) inversion models show the clear superiority of the DD array in imaging the shape, the horizontal dimensions and the vertical extent of the submerged structure. The other arrays either have resistivity signatures that show a vague representation of the feature or the reconstructed model does not show a regular geometric shape that could be attributed to well preserved archaeological relics. It is also obvious that the models from the submerged mode give a stronger resistivity response of the structure because the sensors are directly attached to the sea bottom and thus closer to any potential submerged target. Furthermore, all the models indicate fade remnants of the buried building in the deeper depth slices due to the smoothness constraints imposed to stabilize the inversion and the decreasing resolution with depth of the resistivity survey which does not allow the accurate positioning of the lower limit of the building.

The calculation of the model resolution matrix (R) can provide an extra mathematical tool for the quantitative verification of the above general remarks on the efficiency of each different electrode array. Using linear approximations, the relation between the inverted model resistivity (based on the solution of the smoothness constrained least-squares equation), and the true resistivity is approximated by

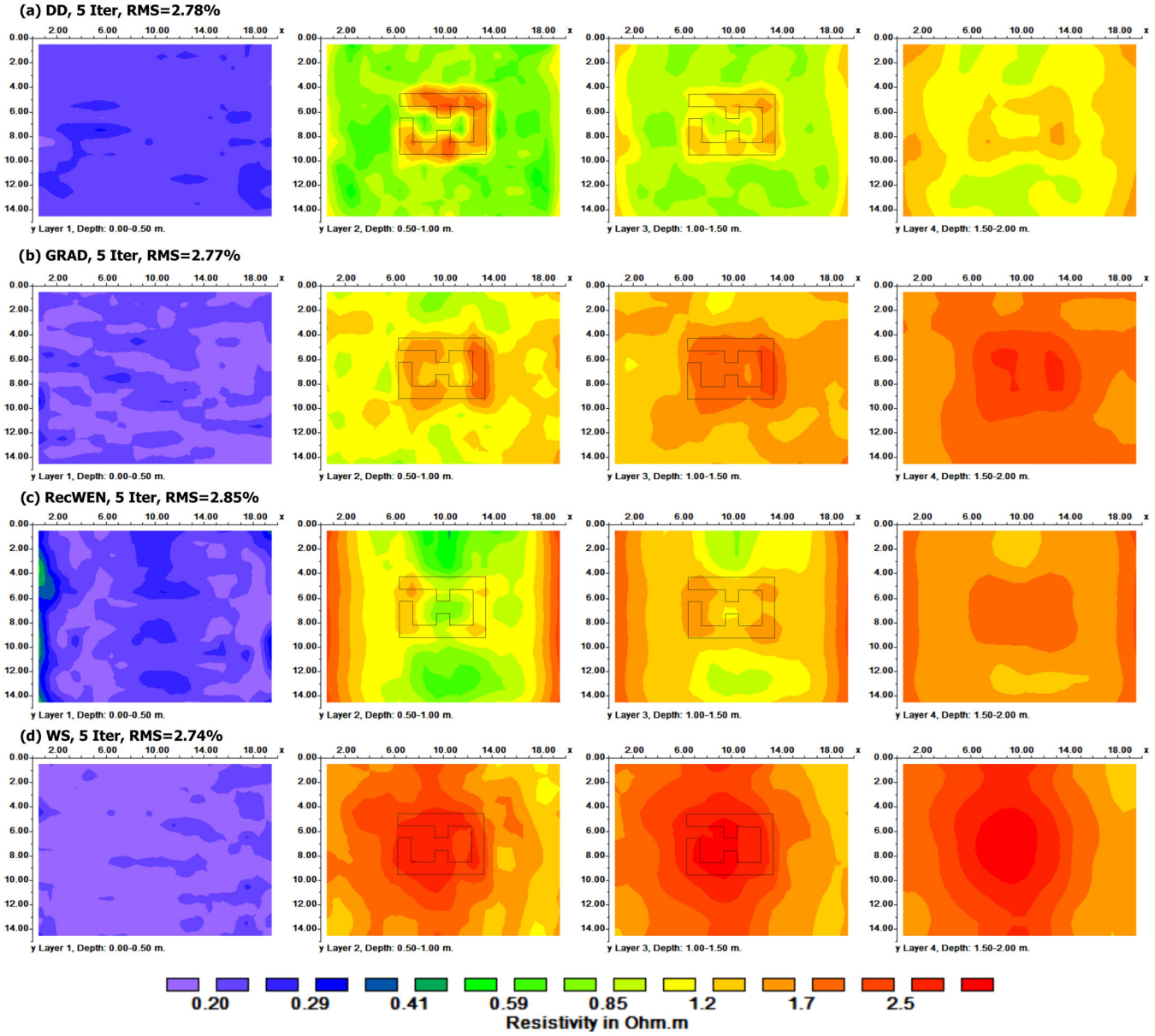

FIGURE 4 Inversion images from the floating survey mode with water layer 0.5 m thick and water resistivity 0.2 Ohm-m. Depth slices extracted from the 3-D inversion models of the synthetic data sets for the floating arrays: (a) dipole–dipole, (b) gradient, (c) reciprocal Wenner and (d) Wenner–Schlumberger [Colour figure can be viewed at wileyonlinelibrary.com]

$x_{model} \approx Rx_{true}$, where $R = (J^TJ + \lambda C^TC)^{-1}J^TJ$ (Friedel, 2003). The model resolution matrix is considered as a filter through which the inversion method attempts to resolve the subsurface resistivity. In the ideal case of perfectly resolved inverted cells, the diagonal elements (R_{ii}) will have the value 1.0 and the off-diagonal 0. In other words, the diagonal elements give the degree of resolution, whereas the off diagonal elements indicate the cross-correlation with the neighbouring model cells. Normally, the resolution is illustrated by plotting the values of the diagonal elements of the R matrix using a value of about 0.05–0.1 (5–10%) as a cutoff value to show non-resolvable regions in the inversion model.

Figure 6 shows the resolution matrix for all the submerged arrays which was calculated for the last iteration of the inversion procedure. The 3-D distribution of the resolution values show that no array carries the necessary information context to resolve any structure below the depth 2 m below the seabed where the resolution values are less than 0.1. However, DD generated relatively higher resolution values which was actually reflected in the respective inversion models and its efficiency to reconstruct the submerged resistivity model (Figure 6a). GRAD and RecWEN have comparable investigation depths reaching no more than 1 m below the seabed, but RecWEN has limited horizontal resolution due to the actual survey pattern and the relative position of current and potential dipoles (Figure 6b,c). The limited resolving power of WS in detecting isolated resistive structures is also verified with the relatively low model resolution values that rapidly decay after the second depth slice (Figure 6d). The

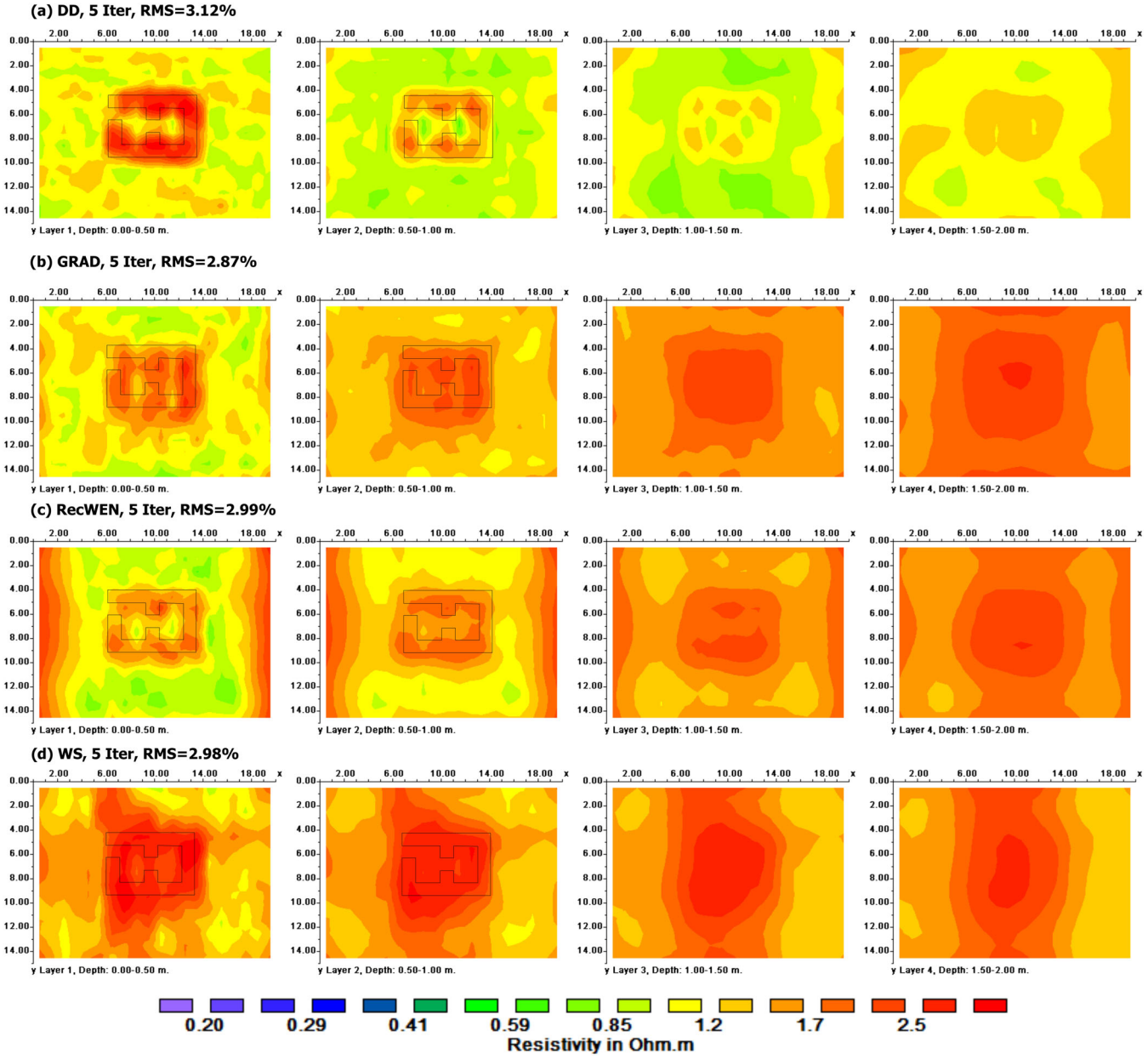

FIGURE 5 Submerged survey mode with water layer 1.0 m thick and resistivity 0.2 Ohm-m (not represented in the respective depth slices). Depth slices extracted from the 3-D inversion models of the synthetic data sets for the submerged arrays: (a) dipole–dipole, (b) gradient, (c) reciprocal Wenner and (d) Wenner-Schlumberger [Colour figure can be viewed at wileyonlinelibrary.com]

respective plots (not shown here) of the model resolution values for the floating arrays also lead to similar conclusions on the resolving capabilities of the different electrode arrays.

3.2 | Effect of water layer thickness

The structural remains were placed within the background resistive medium below sea water layers with variable thickness ranging from 0.5 to 1.5 m. The actual values for the water resistivity and thickness were constrained into the inversion process, and the respective layers are indicated in the inversion reconstructed models (Figure 6a–c). The purpose was to illustrate the effect of the saline environment and investigate the maximum water thickness, to which ERT would be effective in locating isolated resistive targets for the floating survey mode.

In this case, the DD protocol was used for three different water thickness values (0.5, 1.0 and 1.5 m), and the 3-D inversion results are shown in Figure 7a–c. The reconstructed resistivity sections signify the severe decrease of the resolving capability for the floating mode to map the isolated targets with increasing the thickness of the water layer. Although the DD floating inversion model with water layer 0.5 m shows relatively larger RMS error (2.78%), it exhibits the optimum resolution in outlining the submerged structure. If the seawater

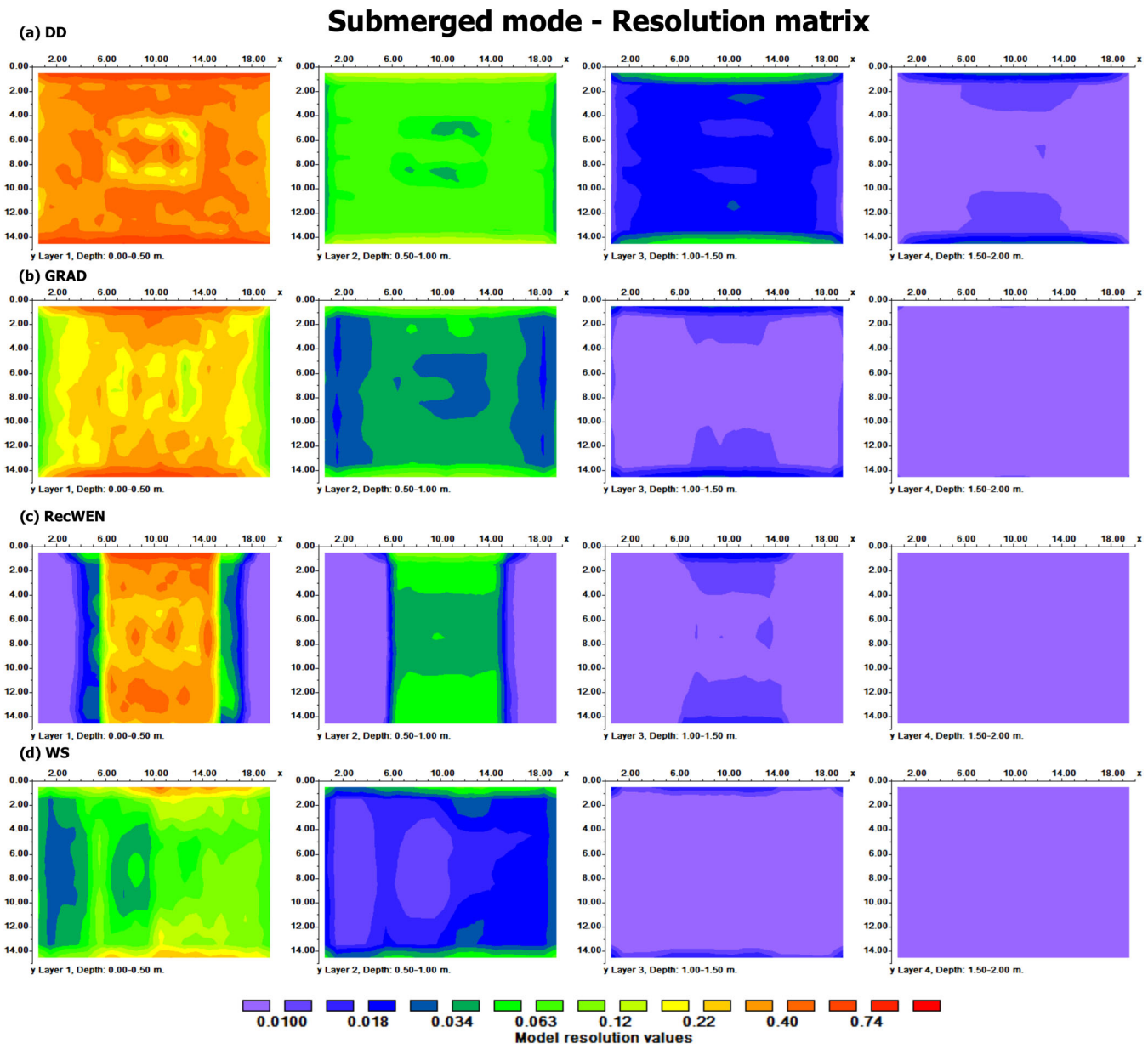

FIGURE 6 Model resolution values for the submerged electrode arrays of (a) dipole–dipole, (b) gradient, (c) reciprocal Schlumberger and (d) Wenner [Colour figure can be viewed at wileyonlinelibrary.com]

layer exceeds the thickness of 0.5 m, it is actually impossible to reconstruct the archaeological body and the tomographic image retrieves information only for the horizontal stratigraphy and the transition from the sea to the background layer.

A similar comparative study was also performed for the submerged mode using the DD array, assuming an uppermost water layer with increasing thickness (Figure 8). The resistivity and the thickness of the saline water layer were accounted during the modelling and inversion of the tomographic data. In all the tested cases, the inversion converged to submerged resistivity models with technically the same RMS error (2.93–2.96%). The depth slices for the different models illustrate the general outline of the building recovering at the same time its vertical continuation within the depth of 0.5–1.0 m below the seabed. Obviously, the resistivity signature of the structure is stronger when the overlying water layer is thinner (Figure 8a,b). However, the modelling results manifest the extraordinary resolving power of the method to locate archaeological structures even in challenging cases with the presence of relatively thicker water layers (Figure 8c,d).

3.3 | Vertical resolution

The vertical resolving capabilities of floating survey modes were investigated using a 0.5 m thick water layer. When the structure is actually buried in the depth slices of 1.0 m–2.0 m below the water

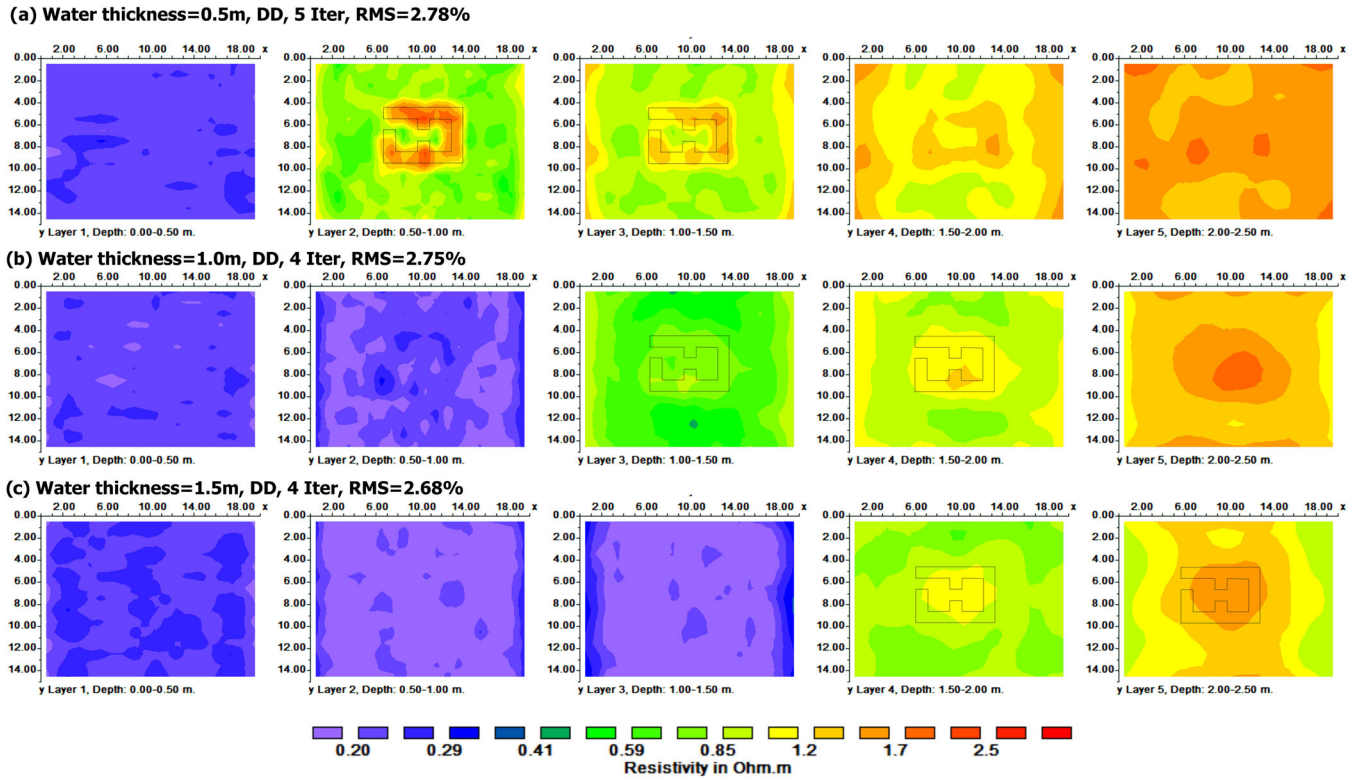

FIGURE 7 Effect of variable thickness of water layer in the resolving capabilities of the floating survey mode using the DD array (a) water thickness: 0.5 m, (b) water thickness 1.0 m and (c) water thickness 1.5 m [Colour figure can be viewed at wileyonlinelibrary.com]

surface, the DD inversion model outlines its general shape but at the same time underestimates its burial depth which is projected closer to the water surface starting to appear in the depth layer of 0.5–1.0 m. In a real situation, this would eventually cause a misleading interpretation regarding the actual burial depth of the upper surface of a specific architectural structure (Figure 9a). The situation is even worse in the case where the feature lies within the layers of 1.5–2.5 m below the sea surface. In such a case, the inversion model is not capable of extracting any valuable information related to the existence of the submerged structure, documenting the critical influence of the water layer in essentially diminishing the vertical resolving power of any floating survey (Figure 9b).

The comparative analysis of the respective submerged resistivity inversion models, assuming an upper water layer with thickness less than 3 m, manifest the efficient vertical resolution of the final ERT images in cases where the top of the submerged structures lies in the depth layer of 0.5–1.0 m below the sea bed (Figure 10a,c). Thicker water layers (>3 m) have progressively larger influence in the inversion depth slices, eventually masking the top of the building for extreme water layers (5 m) and generating compact resistive enclosures in the deeper slices (Figure 10d,e). For the thinner water layer (1 m), the resistivity image shows similar artefacts with the respective floating mode, where the inversion model underestimates the actual burial depth of the feature projecting its upper surface closer to the sea bed (Figure 10a). Furthermore, submerged inversion models actually do not carry the necessary information context to resolve features buried in depth layers more than 1.0 m below the seabed (Figure 10b), regardless the thickness of the upper layer, based on respective modelling and inversion tests using water layer with variable thickness (not shown here).

3.4 | Effect of erroneous measurement of water thickness

The bathymetric variations of the seabed are usually measured with a sonar device which is connected and synchronized with the resistivity instrumentation during the floating or submerged dynamic ERT survey. The compiled digital bathymetry model is then used to extract the thickness of the water layer in different horizontal positions and incorporate this information in the modelling and inversion processing of the tomographic ERT data. Inaccurate measurement of this parameter can risk compromising the quality and the clarity of the final resistivity inversion images. The floating and submerged DD models, respectively, with 0.5 m (Figure 4a) and 1.0 m (Figure 5a) thickness for the water layer, were used to test the effect of erroneous assignment of this parameter in the 3-D inversion results. The seawater resistivity was kept fixed in these examples and equal to 0.2 Ohm-m as it was originally assigned.

Over-estimating (Figure 11a) or under-estimating (Figure 11b) by 50% the actual water depth of 0.5 m for the floating mode had serious effects in the final resistivity image because the actual burial depth of

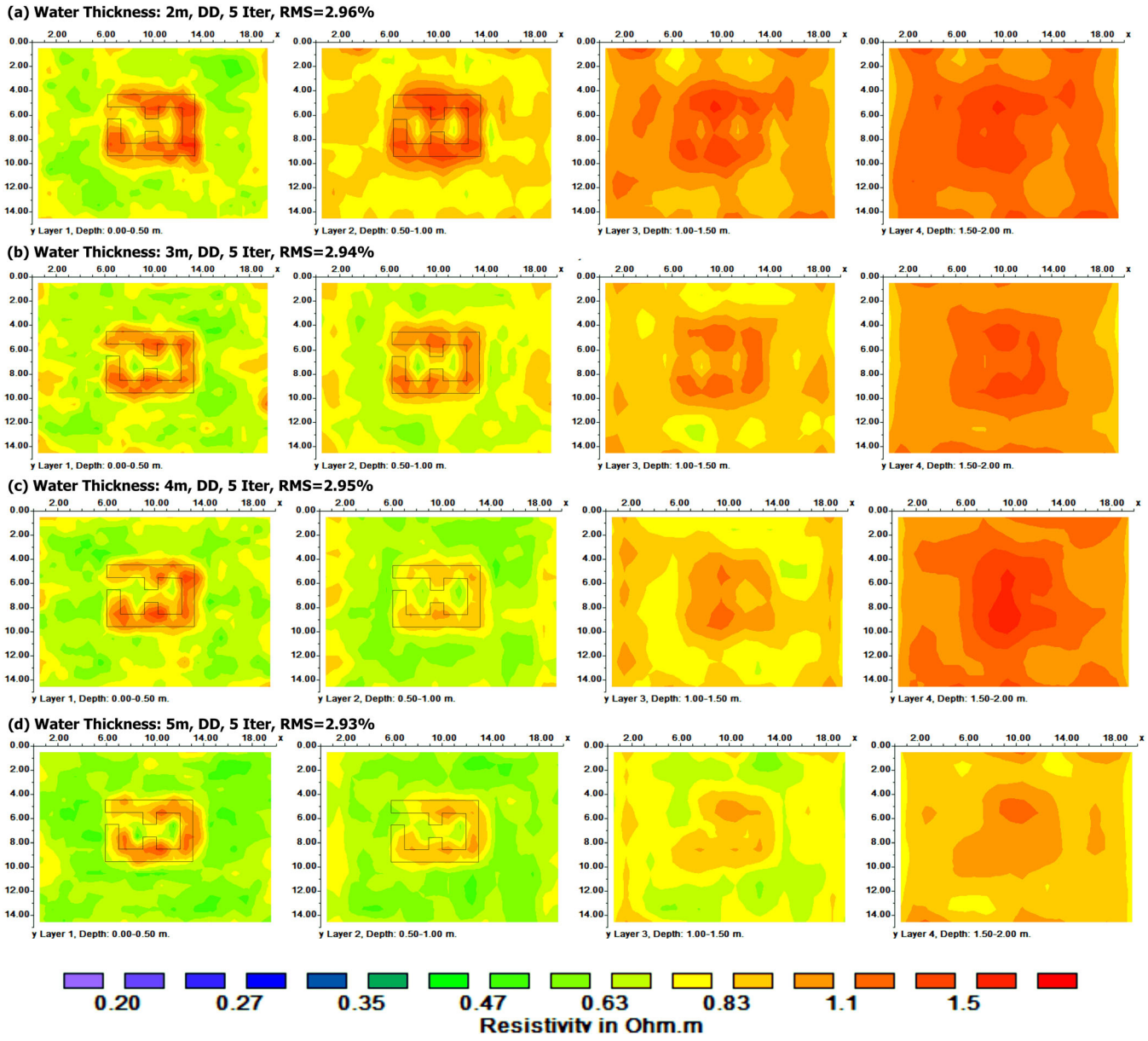

FIGURE 8 Reconstructed 3-D resistivity inversion models of the submerged DD array for water layers with thickness (a) 2 m, (b) 3 m, (c) 4 m and (d) 5 m. The slices refer to the depth below the seabed. The water layer is not shown in the respective depth slices [Colour figure can be viewed at wileyonlinelibrary.com]

the structure is projected deeper to the slice 1.0–1.5 m below the seawater. The distortions are even more severe for the case of the submerged models where measuring the actual thickness of 1 m of the water layer with an error of 50% (Figure 11c,d) masked completely the submerged structure leading to questionable interpretation regarding the actual resistivity distribution.

3.5 | Effect of erroneous estimation in water resistivity

The resistivity of the water layer is also an important physical parameter for the marine archaeological surveys that is measured with a high precision conductivity meter. Once more the floating and submerged DD models, respectively, with 0.5 m (Figure 4a) and 1.0 m (Figure 5a) thickness for the water layer were employed to evaluate the influence of erroneous estimation of the sea water resistivity in the resistivity images. In this case, the water thickness of 0.5 and 1.0 m for the floating and the submerged modes, respectively, remain unchanged.

Figure 12a,b shows that floating inversion models are rather insensitive to an over or underestimation of the seawater resistivity by 50%, because the inversion models have comparable accuracy with resistivity image when the actual water resistivity and thickness values were used. On the other hand, submerged ERT measurements show that inversion artefacts and resistivity distortions appear when assigning erroneous information for the seawater resistivity

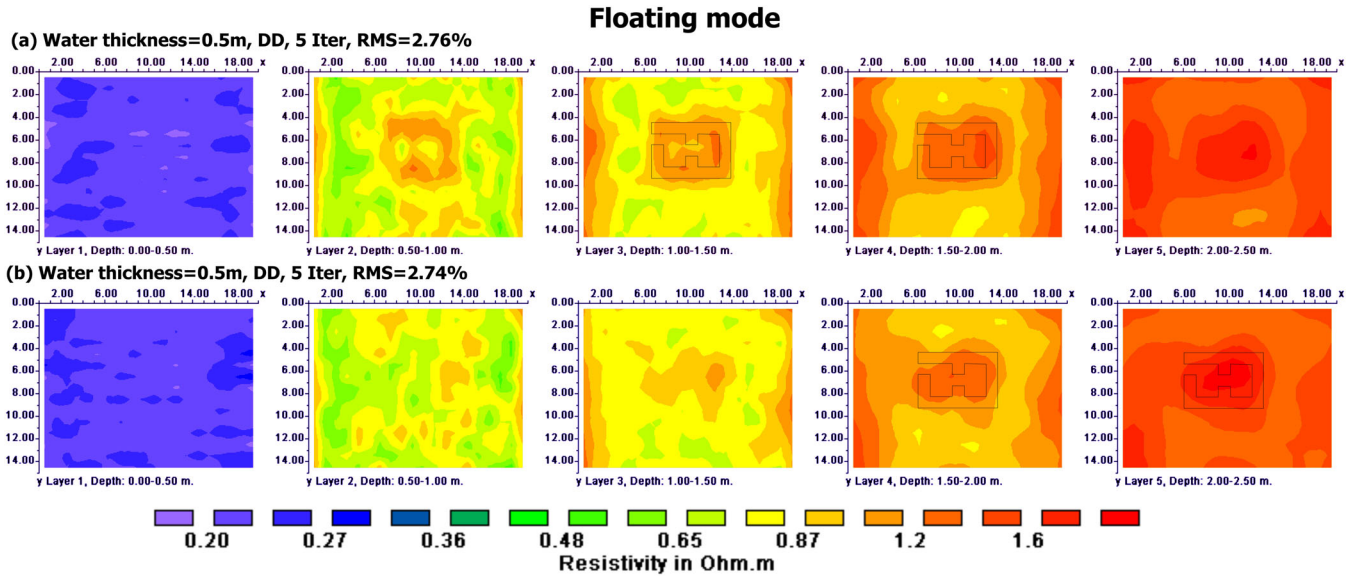

FIGURE 9 Vertical resolving capabilities of a floating ERT survey in locating submerged structures below the sea water surface assuming a constant water layer with thickness 0.5 m [Colour figure can be viewed at wileyonlinelibrary.com]

(Figure 12c,d). The underestimation and overestimation of the water resistivity by at least 20% result in the failure of the method to locate the target. These tests clearly demonstrate the importance of incorporating valid information for the water depth and its resistivity within the inversion procedure in order to reconstruct resistivity models that correspond to the actual subsurface conditions.

4 | FIELD CASE STUDY

The submerged archaeological site of Olous, in the eastern part of Crete Island (Figure 13a), formed the living lab to validate the modelling ERT results with real data from a respective small grid (Figure 13b). Given the limited references to the city in the ancient texts, most of the historical knowledge about its history is derived from the available epigraphic, numismatic and archaeological evidence. A votive pit is currently the most ancient feature and dates the establishment of the settlement to the Archaic period. Regarding the Hellenistic period, the epigraphic evidence attests the existence of a wealthy harbour town in a strategic location. Most of the submerged architectural remains related to buildings of the town have been attributed to that period. Recent in situ underwater surveys and investigations located and mapped part of the currently submerged Hellenistic fortification of Olous including a wall and a potential, defining the southern limit of the harbour (Theodoulou, personal communication).

The Roman Imperial period is attested by cemetery tombs in the surrounding area to the west, by two fragments of inscribed marble statues of the 2nd 3rd century Common Era (CE) and by scattered pottery finds. Parts of the submerged architectural remains are also attributed to this occupation phase of the settlement. A basilica with a mosaic pavement and dedicatory inscriptions dating back to the 7th c. CE manifest the Early Byzantine period. The Venetian period is characterized by the functioning of a large salt pan complex, which was probably established in Byzantine times, and nowadays has been completely abandoned (Theodoulou, personal communication).

The experimental floating dynamic survey was completed in a small part of the submerged archaeological site. The 40 m by 20 m off-shore grid was laid out above a known underwater wall (Figure 13b), in an effort to explore the efficiency of the approach and validate the modelling results. The grid was surveyed with a dense network of 21 parallel ERT transects with 1 m inter-line distance. A cable with 13 equidistant sensors every 1 m was kept floating on the surface of the sea with a number of plastic buoys. The dipole–dipole array with one transmitting dipole close to the instrumentation and 10 receiving dipoles with gradually increasing distance from the current electrode pair was used to capture and store the underwater resistance readings. The sea water resistivity was measured 0.17 Ohm-m with a high precision handheld conductivity meter. The water thickness within the grid, measured with a real time kinematic GNSS system, was fairly constant ranging from 0.46 to 0.54 m with an average value of 0.5 m.

The 13 connectors at the one end of the cable were plugged to a 10-channel electrical resistivity instrument, which was placed inside a floating apparatus along with an external battery, a toughpad and a GPS. The floating device was constructed with a waterproof plastic box, and its interior was divided in compartments using polystyrene for extra isolation and levitation to safely store the instrumentation. The whole apparatus could sustain weight more than 30 kilos. Four elongated wooden sticks with supporting buoys at the edges were placed for stability purposes. The boat's shallow draft (approximately 0.1 m) permitted rapid data acquisition on top of the archaeological relics even in very shallow water depths. This proved to be really useful because the survey could be undertaken in areas very close to the

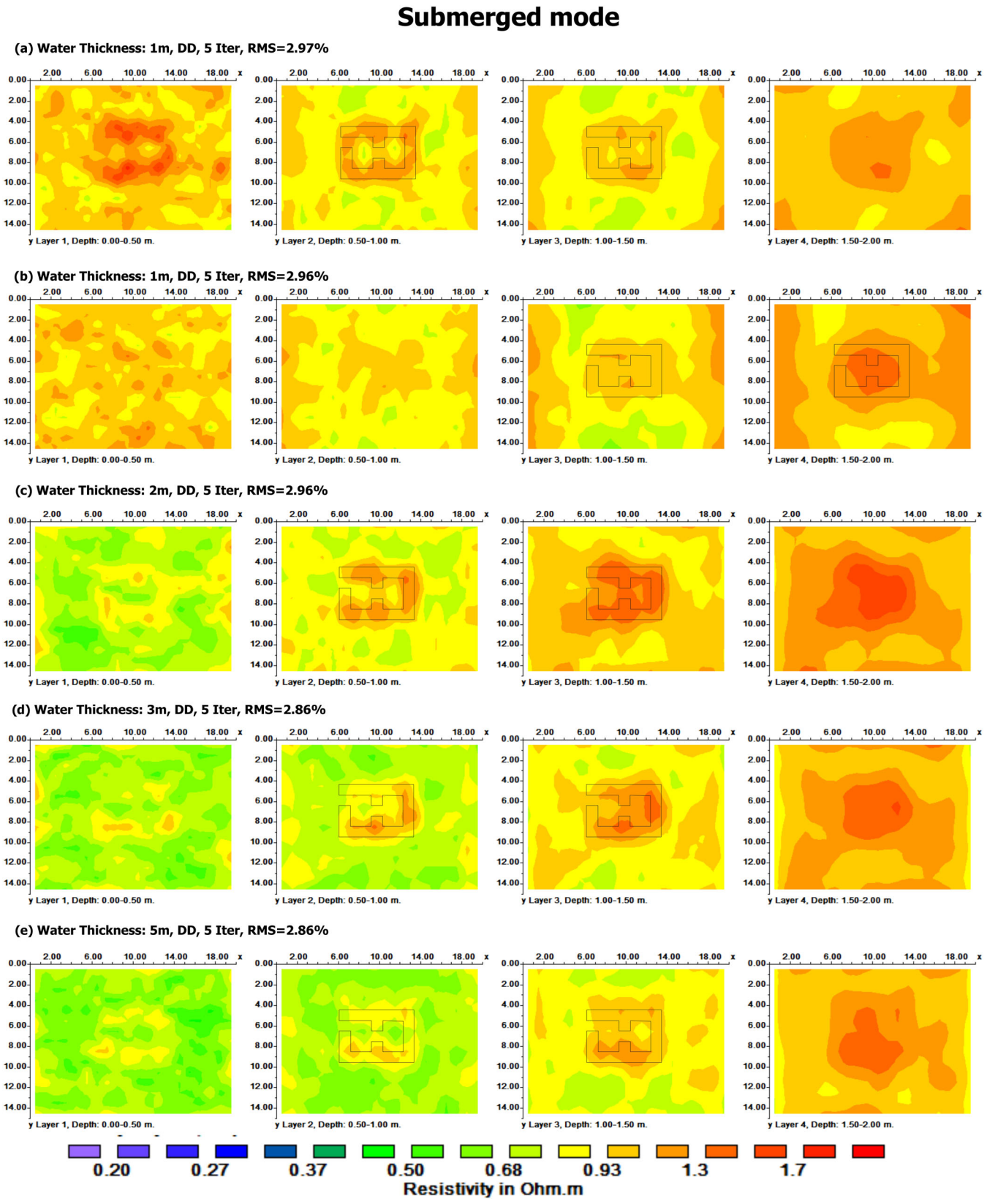

FIGURE 10 Vertical resolving capabilities of a submerged ERT survey in locating structures below the seabed surface assuming a variable water layer with thickness 1.0 m (a, b), 2.0 m (c), 3.0 m (d) and 5.0 m (e) [Colour figure can be viewed at wileyonlinelibrary.com]

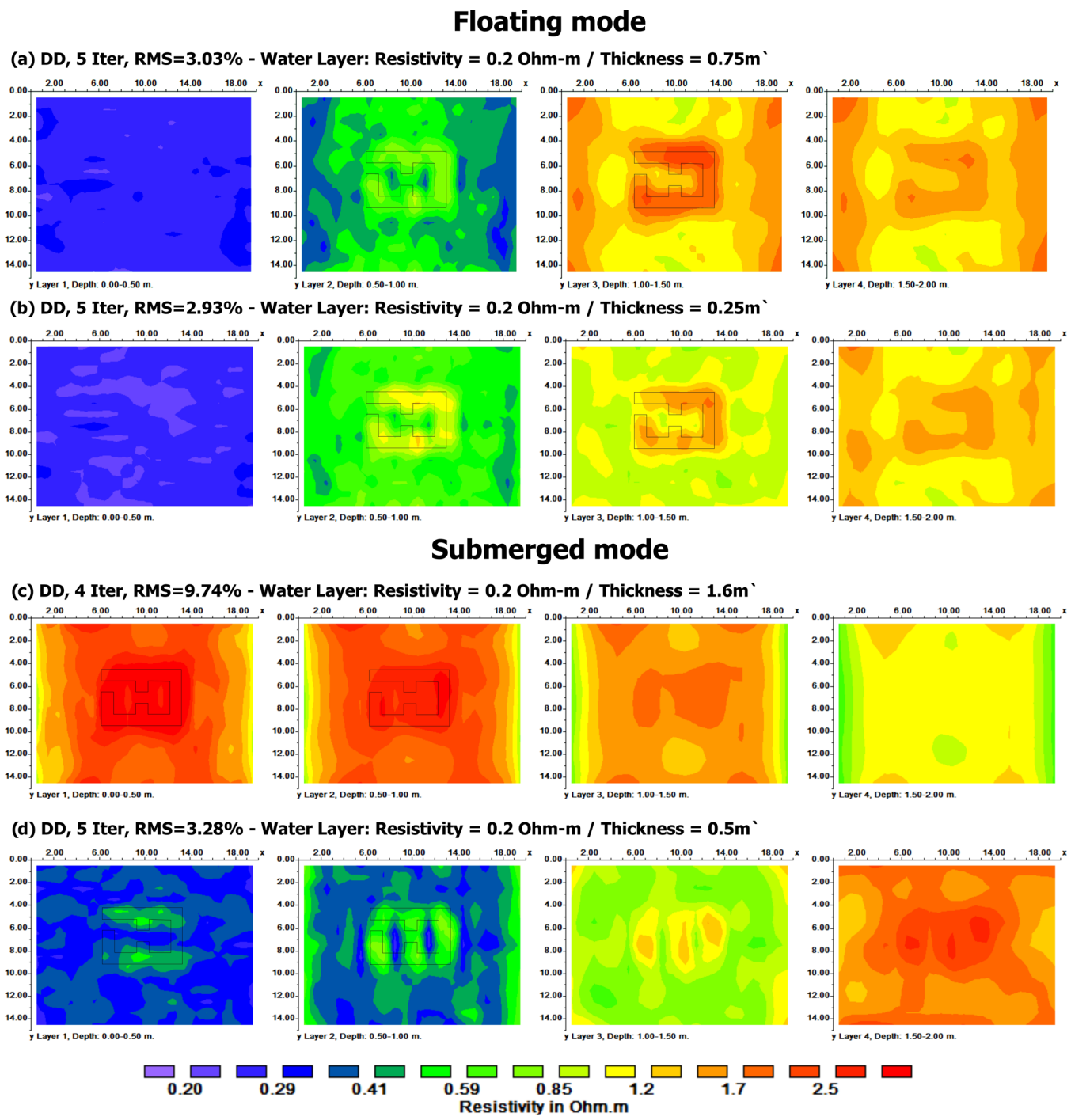

FIGURE 11 Effect of over and under estimating the thickness of water layer in the 3-D inversion resistivity models for the floating and the submerged survey mode with the DD array [Colour figure can be viewed at wileyonlinelibrary.com]

seashore without being hindered by protruding stones or structures on the sea bottom and very close to the water surface (Figure 13c,d).

Figure 14 shows the resistivity models from the surveyed grid in Olous constraining the inversion with the actual, the overestimated and the underestimated parameter values for the thickness and the resistivity of the topmost water layer. A common resistivity color scale was used for all the different depth slices for direct comparison of the respective models which exhibited comparable and relatively low RMS errors (4.22–4.48%). The horizontal slices refer to the depth below the free sea water surface; thus, the first layer corresponding to the water layer was omitted from the presentation for simplicity.

A rectilinear resistive feature characterizes the central section of the grid that is correlated with the continuation of the visible wall crossing the area along the south–north direction. The wall is registered within the second and third depth layers from the sea surface; thus, excluding the water layer, the wall is buried up to 1 m below the

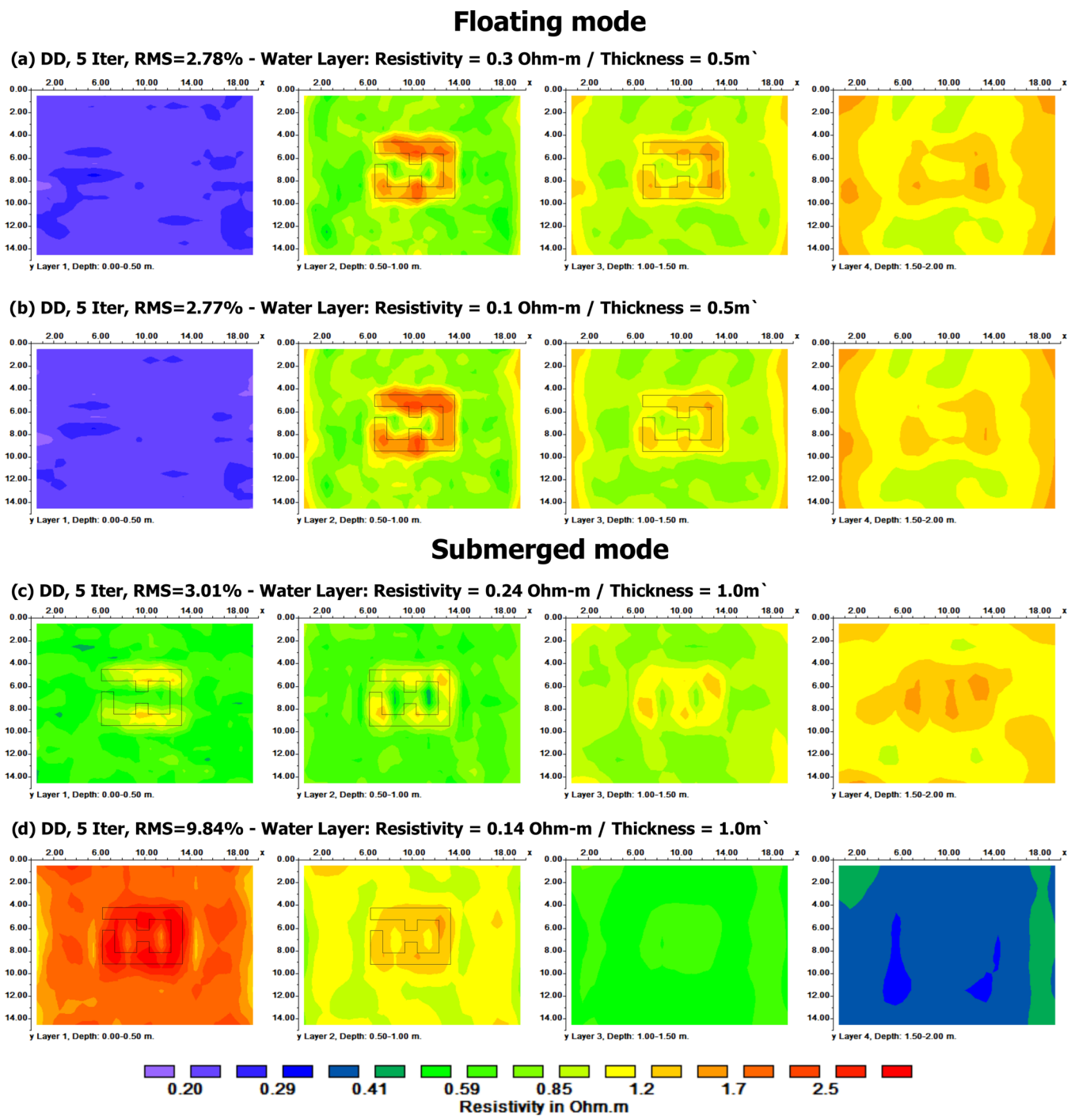

FIGURE 12 Effect of over and under estimating the resistivity of water layer in the 3-D inversion resistivity models for the floating and the submerged survey mode with the DD array [Colour figure can be viewed at wileyonlinelibrary.com]

sea bed. Within the same depth range, the southern and northern edges of the grid respectively, outline two west–east linear resistive segments that are attributed to walls vertically oriented to the main south–north structure. The compact resistive region at the west, which is clearly observed up to the depth layer 2.0–2.5 m below the sea surface (or 1.5–2.0 m below the sea bed), is probably related to a collapsed structure with a relatively poor preservation level or a floor of an older building (Figure 14a).

The underestimation and overestimation of the actual thickness of the water layer for more than 50% resulted in respective inversion artefacts, masking the archaeological structures in the second depth layer and expanding the resistivity range in the deeper layers (Figure 13b,c). On the other hand, the erroneous assignment of the sea water resistivity, even exceeding 50% of the actual value, has a minimal or nonexistent effect on the final 3-D resistivity inversion models (Figure 14d,e).

FIGURE 13 (a) Google Earth satellite image showing the geographic location of the submerged archaeological site of Olous in eastern Crete. (b) Outline of the grid that was laid out in the shallow marine area in Olous to test the efficiency of 3-D floating ERT survey. (c) Integration of the multichannel resistivity instrumentation with a GPS, a toughpad and 12 V battery inside floating box. (d) ERT survey along a single line using plastic buoys to float the cable on surface of the sea water [Colour figure can be viewed at wileyonlinelibrary.com]

The above results document the benefits of the floating survey modes in reconstructing the built cultural material in ultra-shallow offshore environments. The comprehensive knowledge that was gained through the extensive ERT numerical modelling facilitated its successful implementation in the submerged archaeological site of Olous. The results revealed the hidden submerged ancient walls as resistive

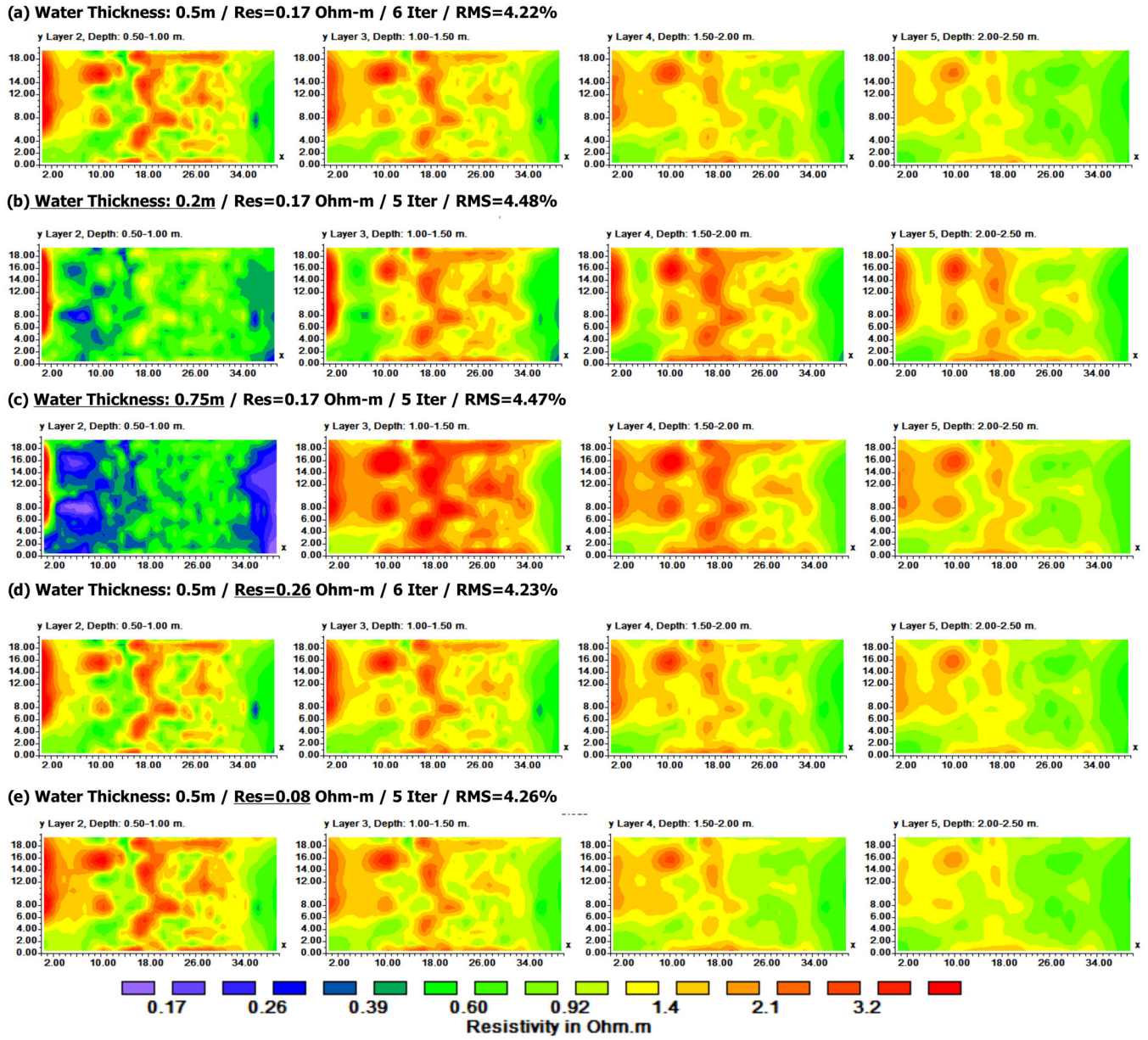

FIGURE 14 Depth slices extracted from the 3-D resistivity inversion model of the floating ERT tomographic data from the grid in the archaeological site of Olous using (a) the actual values for the water resistivity and thickness, (b) underestimating the water thickness, (c) overestimating the water thickness, (d) overestimating the water resistivity and (e) underestimating the water resistivity [Colour figure can be viewed at wileyonlinelibrary.com]

targets within the highly conductive marine context, verifying at the same time the modelling experiment outcomes.

5 | CONCLUSIONS

This work validated the effectiveness of dynamic floating and submerged 3-D ERT survey modes to reconstruct and map complex archaeological structures in ultra-shallow marine environments. This was first approached by creating a generic resistivity model simulating a complex archaeological building within a stratified conductive background environment. The 3-D inversion of the noisy synthetic apparent resistivity tomographic data showed the robustness and superiority of the Dipole–Dipole, in relation to the other tested arrays, to reconstruct the simulated archaeological building both for the floating and the submerged modes.

Numerical modelling results showed that floating and submerged survey modes can be used equally successfully in cases where the thickness of the water layer is less than 1 m. When the water thickness exceeds 1 m, the submerged survey mode should be the primary choice to outline isolated and complex archaeological targets. Constraining the 3-D inversion of the floating and submerged ERT data with the thickness and the resistivity of the seawater layer is important to accurately reconstruct a valid resistivity model below the

seabed. On the other hand, erroneous information overestimating or underestimating about 50% the actual values of the water thickness and resistivity can cause severe distortions in the inverted images leading to inaccurate interpretations.

A dipole–dipole dynamic floating ERT survey was completed within a small marine grid in the submerged archaeological site of Olous in Greece. The 3-D inversion was constrained with the resistivity and thickness of the sea water layer. The respective depth slices outlined a complex building with vertical and horizontal walls reaching the depth of 1 m below the seabed. The inversion of the real data with erroneous a priori information regarding the resistivity and the thickness of the water layer created respective artefacts verifying and enhancing the numerical modelling simulation results.

In general, this work shows the applicability, the potential and the constraints of the 3-D ERT in mapping archaeological structured material, like walls or buildings, in ultra-shallow marine environments. These results can provide the guide to plan the optimum ERT marine survey depending on the characteristics of the potential targets and the respective environmental complexity. Combining these general guidelines with modern and sophisticated 3-D inversion algorithms (M.H. Loke et al., 2020) that minimize the processing time of very large aquatic tomographic data can render ERT a novel tool in the service of archaeological investigation of coastal and shallow marine sites. The general guidelines can be integrated in wider geo-archaeological projects (Beck et al., 2021) to extract quantitative new information about submerged cultural material that is inaccessible to the standard mapping techniques, mapping the vertical stratigraphy and identifying potential geomorphological features that are useful to reconstruct the dynamics and evolution of coastal and shallow submerged archaeological sites.

ACKNOWLEDGEMENTS

This work is supported by the project "Cretan cultural landscapes over the time: highlighting the marine and mountainous environment of Mirabello" with MIS 5028190 that is part of the Priority Axis "Strengthening the competitiveness, innovation and entrepreneurship of Crete" of the Operational Programme "Crete 2014–2020," and it is co-financed by the European Regional Development Fund.

CONFLICT OF INTEREST

The authors declare no conflict of interest.

DATA AVAILABILITY STATEMENT

The data that support the findings of this study are available from the corresponding author upon reasonable request.

ORCID

Nikos Papadopoulos https://orcid.org/0000-0003-1748-5844

REFERENCES

Abdullah, F. M., Loke, M. H., Nawawi, M., & Abdullah, K. (2019). Improving the resolution of 3-D resistivity surveys along the perimeter of a confined area using optimized arrays. *Pure and Applied Geophysics*, *176*, 1701–1715. https://doi.org/10.1007/s00024-018-2061-0

Al-Saadi, O. S., Schmidt, V., Becken, M., & Fritsch, T. (2018). Very-high-resolution electrical resistivity imaging of buried foundations of a Roman villa near Nonnweiler, Germany. *Archaeological Prospection*, *25*, 209–218. https://doi.org/10.1002/arp.1703

Arato, A., Piro, S., & Sambuelli, L. (2015). 3D inversion of ERT data on an archaeological site using GPR reflection and 3D inverted magnetic data as a priori information. *Near Surface Geophysics*, *13*, 545–556. https://doi.org/10.3997/1873-0604.2015046

Baumgartner, F. (1996). A new method for geoelectrical investigations underwater. *Geophysical Prospecting*, *44*, 71–98. https://doi.org/10.1111/j.1365-2478.1996.tb00140.x

Beck, J., Koutsoumba, D., Sakellariou, D., Surdez, M., Anselmetti, F., Papadopoulos, N., Morfis, I., Panagiotopoulos, I., Rousakis, G., Oikonomou, D., Simyrdanis, K., Cantoro, G., Argyriou, A., Emery, P. B., Krijnen, A., & Tsampouraki-Kraounaki, K. (2021). Searching for Neolithic sites in the bay of Kiladha. *Greece*, *Quaternary International*, *584*, 129–140. https://doi.org/10.1016/j.quaint.2020.12.025

Bouchette, G., Church, P., McFee, J. E., & Adler, A. (2014). Imaging of compact objects buried in underwater sediments using electrical impedance tomography. *IEEE Transactions on Geoscience and Remote Sensing*, *52*, 1407–1417. https://doi.org/10.1109/TGRS.2013.2250982

Brinon, C., Simon, F., & Tabbagh, A. (2012). Rapid 1D/3D inversion of shallow resistivity multipole data: Examples in archaeological prospection. *Geophysics*, *77*, E193–E201. https://doi.org/10.1190/geo2011-0309.1

Carretero, S., Rapaglia, J., Perdomo, S., Albino Martínez, C., Rodrigues Capítulo, L., Gómez, L., & Kruse, E. (2019). A multi-parameter study of groundwater–seawater interactions along Partido de La costa, Buenos Aires Province, Argentina. *Environmental Earth Sciences*, *78*, 513. https://doi.org/10.1007/s12665-019-8532-5

Chen, R., Tian, G., Zhao, W., Wang, Y., & Yang, Q. (2018). Electrical resistivity tomography with angular separation for characterization of burial mounds in southern China. *Archaeometry*, *60*, 1122–1134. https://doi.org/10.1111/arcm.12379

Cifuentes-Nava, G., Sánchez-Vázquez, V., Chávez-Segura, R. E., Tejero-Andrade, A., & Hernández-Quintero, J. E. (2013). Electrical resistivity tomography 3D study in Pahñú archaeological site, Central México. 26th symposium on the application of geophysics to engineering and environmental problems 2013. *SAGEEP*, *2013*, 570–573.

Clemenence, H., Marc, P., Veronique, D., & Toihir, A. (2017). Monitoring an artificial tracer test within streambed sediments with time lapse underwater 3D ERT. *Journal of Applied Geophysics*, *139*, 158–169. https://doi.org/10.1016/j.jappgeo.2017.02.003

Dabas, M. (2008). Theory and practice of the new fast electrical imaging system ARP©. In S. Campana & S. Piro (Eds.), *Seeing the unseen: Geophysics and landscape archaeology* (1st ed.) (pp. 105–126). London: CRC Press.

Dahlin, T., & Loke, M. H. (2018). Underwater ERT surveying in water with resistivity layering with example of application to site investigation for a rock tunnel in Central Stockholm. *Near Surface Geophysics*, *16*, 230–237. https://doi.org/10.3997/1873-0604.2018007

deGroot-Hedlin, C., & Constable, S. (1990). Occam's inversion to generate smooth, two-dimensional models from magnetotelluric data. *Geophysics*, *55*, 1613–1624. https://doi.org/10.1190/1.1442813

Di Fiore, B., Mauriello, P., Monna, D., & Patella, D. (2002). Examples of application of tensorial resistivity probability tomography to architectonic and archaeological targets. *Annals of Geophysics*, *45*, 417–430.

Drahor, M. G., Göktürkler, G., Berge, M. A., Kurtulmuş, T. Ö., & Tuna, N. (2007). 3-D resistivity imaging from an archaeological site in South-Western Anatolia, Turkey: A case study. *Near Surface Geophysics*, *5*, 195–201. https://doi.org/10.3997/1873-0604.2006031

Fediuk, A., Wilken, D., Thorwart, M., Wunderlich, T., Erkul, E., & Rabbel, W. (2020). The applicability of an inverse schlumberger array

for near-surface targets in shallow water environments. *Remote Sensing*, *12*, 2132.

Friedel, S. (2003). Resolution, stability and efficiency of resistivity tomography estimated from a generalized inverse approach. *Geophysical Journal International*, *153*, 305–316. https://doi.org/10.1046/j.1365-246X.2003.01890.x

Gündogdu, N. Y., & Candansayar, M. E. (2018). Three-dimensional regularized inversion of DC resistivity data with different stabilizing functionals. *Geophysics*, *83*, E399–E407. https://doi.org/10.1190/geo2017-0558.1

Imaduddi, I., Srigutomo, W., & Mustopa, E. J. (2019). Development of data acquisition instrumentation and inversion system for earth resistivity survey in a smart integrated system. *Journal of Physics: Conference Series*, *1204*(1), 012122.

Kuras, O., Meldrum, P. I., Beamish, D., Ogilvy, R. D., & Lala, D. (2007). Capacitive resistivity imaging with towed arrays. *Journal of Environmental and Engineering Geophysics*, *12*, 267–279. https://doi.org/10.2113/JEEG12.3.267

Kuras, O., Swift, R., Uhlemann, S., Wilkinson, P., Inauen, C., Meldrum, P., 2018. Geoelectrical imaging of concealed objects with capacitive sensor arrays. 24th European Meeting of Environmental and Engineering Geophysics, DOI: https://doi.org/10.3997/2214-4609.201802649

Kwon, H., Kim, J. H., Ahn, H. Y., Yoon, J. S., Kim, K. S., Jung, C. K., Lee, S. B., & Uchida, T. (2005). Delineation of a fault zone beneath a riverbed by an electrical resistivity survey using a floating streamer cable. *Exploration Geophysics*, *36*, 50–58. https://doi.org/10.1071/EG05050

Lagabrielle, R. (1983). The effect of water on direct current resistivity measurement from sea, river or lake floor. *Geoexploration*, *21*, 165–170. https://doi.org/10.1016/0016-7142(83)90006-6

Lee, H., Jung, H.-K., Cho, S.-H., Kim, Y., Rim, H., & Lee, S. K. (2018). Real-time localization for underwater moving object using precalculated DC electric field template. *IEEE Transactions on Geoscience and Remote Sensing*, *56*, 5813–5823.

Loddo, F., Ranieri, G., Piroddi, L., Trogu, A., Cogoni, M., 2016. On the use of electrical resistivity tomography in shallow water marine environment for archaeological research, 22nd European Meeting of Environmental and Engineering Geophysics, Near Surface Geoscience *2016*.

Loke, M. H. (2014). *RES3DMODx64: 3-D resistivity & IP forward modeling using the finite-difference and finite-element methods*. Geotomo Software, Malaysia: User's Manual.

Loke, M. H., 2017. RES3DINVx64: Rapid 3-D resistivity & IP inversion using the least squares method, user's manual, Geotomo Software, Malaysia.

Loke, M. H., & Barker, R. D. (1996). Practical techniques for 3-D resistivity surveys and data inversion. *Geophysical Prospecting*, *44*, 499–523. https://doi.org/10.1111/j.1365-2478.1996.tb00162.x

Loke, M. H., Chambers, J. E., Rucker, D. F., Kuras, O., & Wilkinson, P. B. (2013). Recent developments in the direct-current geoelectrical imaging method. *Journal of Applied Geophysics*, *95*, 135–156. https://doi.org/10.1016/j.jappgeo.2013.02.017

Loke, M. H., Dahlin, T., Rucker, D., 2019. The inversion of 2-D and 3-D resistivity data from surveys in aquatic areas, EAGE-GSM 2nd Asia Pacific Meeting on Near Surface Geoscience and Engineering.

Loke, M. H., & Lane, J. W. L. Jr. (2004). Inversion of data from electrical resistivity imaging surveys in water-covered areas. *Exploration Geophysics*, *35*, 266–271. https://doi.org/10.1071/EG04266

Loke, M. H., Papadopouslos, N., Wilkinson, P. B., Oikonomou, D., Simyrdanis, K., & Rucker, D. F. (2020). The inversion of data from very large three-dimensional electrical resistivity tomography mobile surveys. *Geophysical Prospecting*, *68*, 2579–2597. https://doi.org/10.1111/1365-2478.13008

Mauriello, P., Monna, D., & Patella, D. (1998). 3-D geoelectric tomography and archaeological applications. *Geophysical Prospecting*, *46*, 543–570. https://doi.org/10.1046/j.1365-2478.1998.00102.x

Orlando, L. (2013). Some considerations on electrical resistivity imaging for characterization of waterbed sediments. *Journal of Applied Geophysics*, *95*, 77–89. https://doi.org/10.1016/j.jappgeo.2013.05.005

Osella, A., Vega, M., & Lascano, E. (2005). 3-D electrical imaging of archaeological sites using electrical and electromagnetic method. *Geophysics*, *70*(4), 101–107.

Panissod, C., Dabas, A., Jolivet, A., & Tabbagh, A. (1997). A novel mobile multipole system (MUCEP) for shallow (0-3m) geoelectrical investigation: The "Vol-de-canards" array. *Geophysical Prospecting*, *45*, 983–1002. https://doi.org/10.1046/j.1365-2478.1997.650303.x

Papadopoulos, N., 2019. Reconstructing the natural and cultural environment with electrical resistivity tomography: Advances and applications in eastern Mediterranean the last decade. AGUFM, NS42A-12.

Papadopoulos, N. G., Tsokas, G. N., Dabas, M., Yi, M.-J., Kim, J.-H., & Tsourlos, P. (2009). Three-dimensional inversion of automatic resistivity profiling data. *Archaeological Prospection*, *16*, 267–278. https://doi.org/10.1002/arp.361

Papadopoulos, N. G., Tsourlos, P., Papazachos, C., Tsokas, G. N., Sarris, A., & Kim, J.-H. (2011). An algorithm for the fast 3-D resistivity inversion of surface electrical resistivity data: Application on imaging buried antiquities. *Geophysical Prospection*, *59*, 557–575.

Papadopoulos, N. G., Tsourlos, P., Tsokas, G. N., & Sarris, A. (2006). 2D and 3-D resistivity imaging in archaeological site investigation. *Archaeological Prospection*, *13*, 163–181.

Papadopoulos, N. G., Tsourlos, P., Tsokas, G. N., & Sarris, A. (2007). Efficient ERT measuring and inversion strategies for 3-D imaging of buried antiquities. *Near Surface Geophysics*, *5*, 349–362.

Papadopoulos, N. G., Yi, M. Y., Kim, J.-H., Tsokas, G. N., & Tsourlos, P. (2010). Geophysical investigation of tumuli by means of surface 3-D electrical resistivity tomography. *Journal of Applied Geophysics*, *70*, 192–205.

Passaro, S. (2010). Marine electrical resistivity tomography for shipwreck detection in very shallow water: A case study from Agropoli (Salerno, southern Italy). *Journal of Archaeological Science*, *37*, 1989–1998. https://doi.org/10.1016/j.jas.2010.03.004

Psomiadis, D., Tsourlos, P., & Albanakis, K. (2009). Electrical resistivity tomography mapping of beachrocks: Application to the island of Thassos (N. Greece). *Environmental Earth Sciences*, *59*, 233–240.

Rucker, D. F., & Noonan, G. E. (2013). Using marine resistivity to map geotechnical properties: A case study in support of dredging the Panama Canal. *Near Surface Geophysics*, *11*, 625–637. https://doi.org/10.3997/1873-0604.2012017

Rucker, D. F., Noonan, G. E., & Greenwood, W. J. W. (2011). Electrical resistivity in support of geological mapping along the Panama Canal. *Engineering Geology*, *117*, 121–133.

Schlumberger, C. (1912). *Premières expériences. Carte des courbes équipotentielles, tracées au courant continu Val-Richer (Calvados). Août-Septembre 1912. Ref 4717*. Calvados, France: Musée de Crèvecoeur en Auge.

Simyrdanis, K., Moffat, I., Papadopoulos, N., Kowlessar, J., & Bailey, M. (2018). 3D mapping of the submerged crowie barge using electrical resistivity tomography. *International Journal of Geophysics*, *2018*, 6480565.

Simyrdanis, K., Papadopoulos, N., & Cantoro, G. (2016). Shallow offshore archaeological prospection with 3-D electrical resistivity tomography: The case of Olous (modern Elounda), Greece. *Remote Sensing*, *8*, 897. https://doi.org/10.3390/rs8110897

Simyrdanis, K., Papadopoulos, N., Kim, J.-H., Tsourlos, P., & Moffat, I. (2015). Archaeological investigations in the shallow seawater environment with electrical resistivity tomography. *Near Surface Geophysics*, *13*, 601–611. https://doi.org/10.3997/1873-0604.2015045

Stummer, P., Maurer, H., & Green, A. G. (2004). Experimental design: Electrical resistivity data sets that provide optimum subsurface information. *Geophysics*, *69*, 120–139. https://doi.org/10.1190/1.1649381

Sumintadireja, P., & Irawan, D. (2016). Static electrode DC resistivity measurement at surface water for pond subsurface layer imaging. *IOP Conference Series: Earth and Environmental Science*, *29*, 012024. https://doi.org/10.1088/1755-1315/29/1/012024

Szalai, S., Varga, M., Novák, A., & Szarka, L. (2011). Non-conventional geoelectric arrays—Practical results of the OTKA project K49604. *Acta Geodaetica et Geophysica Hungarica*, *46*, 379–390. https://doi.org/10.1556/AGeod.46.2011.4.1

Tassis, G. A., Tsourlos, P. I., & Ronning, J. S. (2020). Detection and characterization of fracture zones in bedrock in marine environment: Possibilities and limitations. *Near Surface Geophysics*, *18*, 91–103. https://doi.org/10.1002/nsg.12086

Tejero-Andrade, A., Cifuentes, G., Chávez, R. E., López-González, A. E., & Delgado-Solórzano, C. (2015). L- and corner-arrays for 3D electric resistivity tomography: An alternative for geophysical surveys in urban zones. *Near Surface Geophysics*, *13*, 355–367. https://doi.org/10.3997/1873-0604.2015015

Tsourlos, P., Papadopoulos, N., Yi, M.-J., Kim, J.-H., & Tsokas, G. (2014). Comparison of measuring strategies for the 3-D electrical resistivity imaging of tumuli. *Journal of Applied Geophysics*, *101*, 77–85. https://doi.org/10.1016/j.jappgeo.2013.11.003

Vafidis, A., Sarris, A., Sourlas, G., Ganiatsos, Y. 1999. Two and three-dimensional electrical tomography investigations in the archaeological site of Itanos, Crete, Greece. Second Balkan Geophysical Congress and Exhibition, Istanbul, Turkey, July, 5-9, 1999.

Yang, C. H., You, J. I., & Lin, C. (2002). Delineating lake bottom structure by resistivity image profiling on water surface. *Terrestrial Atmospheric and Oceanic Sciences.*, *13*, 39–52. https://doi.org/10.3319/TAO.2002.13.1.39(T)

Yilmaz, S., Balkaya, Ç., Çakmak, O., & Oksum, E. (2019). GPR and ERT explorations at the archaeological site of Kılıç village (Isparta, SW Turkey). *Journal of Applied Geophysics*, *170*, 103859. https://doi.org/10.1016/j.jappgeo.2019.103859

How to cite this article: Papadopoulos, N., Oikonomou, D., Simyrdanis, K., & Heng, L. M. (2021). Practical considerations for shallow submerged archaeological prospection with 3-D electrical resistivity tomography. *Archaeological Prospection*, 1–21. https://doi.org/10.1002/arp.1841